JOURNAL OF COMPUTATIONAL PHYSICS **124,** 324–336 (1996)
ARTICLE NO. 0063

A Pseudospectral Chebychev Method for the 2D Wave Equation with Domain Stretching and Absorbing Boundary Conditions

ROSEMARY RENAUT* AND JOCHEN FRÖHLICH†

*Department of Mathematics, Arizona State University, Tempe, Arizona 85287-1804 and †Konrad-Zuse-Zentrum für Informationstechnik, Heilbronner Strasse 10, 10711 Berlin-Wilmersdorf, Germany

Received February 21, 1995

In this paper we develop a method for the simulation of wave propagation on artificially bounded domains. The acoustic wave equation is solved at all points away from the boundaries by a pseudospectral Chebychev method. Absorption at the boundaries is obtained by applying one-way wave equations at the boundaries, without the use of damping layers. The theoretical reflection coefficient for the method is compared to theoretical estimates of reflection coefficients for a Fourier model of the problem. These estimates are confirmed by numerical results. Modification of the method by a transformation of the grid to allow for better resolution at the center of the grid reduces the maximum eigenvalues of the differential operator. Consequently, for stability the maximum timestep is $O(1/N)$ as compared to $O(1/N^2)$ for the standard Chebychev method. Therefore, the Chebychev method can be implemented with efficiency comparable to that of the Fourier method. Moreover, numerical results presented demonstrate the superior performance of the new method.

1. INTRODUCTION

This paper describes and evaluates a technique for the application of artificial absorbing boundary conditions, in conjunction with pseudospectral methods, for the simulation of acoustic wave propagation. Typical numerical simulations of wave propagation phenomena require a technique to eliminate spurious reflections from the numerical boundaries of the domain. Finite difference solutions achieve this by the imposition of artificial boundary conditions which have been designed to absorb incident waves at the boundary; see for example, [5, 7, 8, 10, 11, 19]. Alternative approaches require the inclusion of a damping region around the physical region, in which the solution is gradually damped to zero [4]. Kosloff and Kosloff [15] have adapted this technique for the pseudospectral Fourier method applied to forward modelling so that the acoustic wave equation is modified by a damping term, non-zero only in a damping region at the boundary. These methods have been used for a wide variety of applications; see for example the recent papers by Kosloff *et al.* [17] and Tessmer and Kosloff [22]. The solution, however, maintains the periodicity induced by the Fourier method, and therefore the damping layer has to be large enough to prevent reentrant waves at the physical boundary. Hence the approach is not only costly in terms of memory requirements but also it is not very flexible. In particular, the appropriate damping layer must be determined for each problem solved, dependent on location of the initial signal and the time interval over which a solution is required. The method proposed here, in which a one-way wave equation is applied at the boundary, avoids these problems by removing both periodicity and damping layers. Moreover, the high-accuracy advantage of the pseudospectral spatial approximation is maintained by the use of a Chebychev pseudospectral formulation. We note that the new technique is similar to a method proposed by Kopriva [3], for the linearized gas dynamics equations, and by Carcione [3] for the solution of the 2D wave equation recast as a first-order linear hyperbolic system.

In Section 2 of the paper the absorbing boundary formulation for the solution of the acoustic wave problem is presented. The wave equation is solved at all points away from the boundary by a Chebychev pseudospectral method, in which the spatial derivatives are approximated via a Chebychev expansion of the solution. The absorbing boundaries are modelled by first-order one-way wave equations (OWWEs). The spatial derivatives of these boundary equations are also approximated using the same Chebychev expansions. Integration in time is obtained by an implicit Crank–Nicholson method at the boundaries and a standard second-order discretization in time at the interior points.

The modified Chebychev method (see [16]) which allows better resolution at the center of the grid, is extended to second-order differential operators in space. Therefore, in Section 3, we also present graphs of the eigenvalue distributions of the modified differentiation operators. The spectral radii of these operators suggest that integration can proceed with timesteps $O(1/N)$ instead of $O(1/N^2)$. This is confirmed by numerical experiment.

In Section 4 the theoretical reflection coefficient for the

0021-9991/96 $18.00

acoustic wave equation modified by OWWEs applied in damping layers near the boundaries is compared with estimates of the reflection coefficient for the modified equation with damping layer, presented in [15]. Note, that for normally incident waves, the reflection coefficient of the first-order OWWE is identically zero. Thus our comparison suggests a problem inherent in the pseudospectral Fourier method but lacking in the Chebychev formulation: the damping layer has to be very carefully designed with respect to its thickness and the shape of its damping function in order to prevent both reflected and reentrant waves over the time period of the simulation.

We conclude with a performance evaluation of the Chebychev pseudospectral method for acoustic wave simulation in which the acoustic wave equation is solved at all points, except those at the boundary, for which OWWEs are used. The results are compared with the pseudospectral Fourier formulation [14] applied, as in [15], to their modified equation. Our results verify the superior performance of the new method and confirm that the modified Chebychev method can be implemented with a timestep restriction $O(1/N)$, equivalent to that used in the Fourier method.

The Chebychev formulation combined with the first-order OWWE offers a flexibility not found in the Fourier method. In particular, the absorbing boundary condition need only be applied at one boundary, thus opening up the possibility of the incorporation of absorbing boundaries into problems with complicated geometries for which the need to do a domain decomposition eliminates the ability to use periodic solution techniques. Furthermore, the $O(1/N)$ timestep restriction means that the overall cost is less than that for the Fourier method because the fast Fourier transform (FFT) can still be applied for the calculation of the derivatives and at the same time the numerical domains are reduced as compared to those employed in the Fourier method.

2. THE METHOD

2.1. *OWWE and Spatial Discretization*

The pseudospectral Chebychev method (see [2]) is employed for the solution of the acoustic wave equation

$$u_{tt} = c^2(u_{xx} + u_{yy}), \tag{2.1}$$

on the artificially bounded domain $D = \{(x, y) : 0 < x < 1, 0 < y < 1\}$. The solutions $u = u(x, y, t)$ of (2.1) are superpositions of plane waves which propagate in every direction in two dimensions. Contributions which travel towards the boundary of the domain D have to leave this domain freely, without reflection at the boundaries. For the solution of (2.1) by finite-difference methods this requirement is achieved by the imposition of the appropriate one-way wave equations at the boundaries; see [5, 7, 8, 10, 11, 19]. The lowest order one-way wave equation which is effective is given by

$$\left(\frac{\partial}{\partial t} - c\frac{\partial}{\partial x}\right) u(x, y, t) = 0, \tag{2.2}$$

at the $x = 0$ boundary. This equation allows for the complete absorption of all waves incident normally to the boundary at $x = 0$. For waves incident other than normally the reflection coefficient is small for near-normal waves but increases to 1 for waves of glancing incidence at the boundary. The reflection can be reduced by applying either higher-order one-way wave equations [19] or operators of the kind (2.2) superposed to give absorption or some chosen set of incident waves [11]. In this paper we consider (2.1) in conjunction with (2.2). The results presented demonstrate that (2.2) is effective in absorbing most outgoing waves.

Equations of type (2.2) can be solved together with (2.1) in such a way that the appropriate OWWEs dominate near the boundary without modifying the solution on the inner region. This formulation resembles the one considered in [15] and replaces the acoustic wave equation by the modified equation

$$\begin{aligned}(1 - (\varepsilon_1 + \varepsilon_2))(1 - (\varepsilon_3 + \varepsilon_4))(u_{tt} - c^2(u_{xx} + u_{yy})) \\ = \varepsilon_1(u_t + cu_x) + \varepsilon_2(u_t - cu_x) \\ + \varepsilon_3(u_t + cu_y) + \varepsilon_4(u_t - cu_y).\end{aligned} \tag{2.3}$$

Here the functions ε_i are functions of x and y, chosen so that the appropriate one-way wave equation dominates at each boundary. The width of the damping layer at a given boundary then depends on the appropriate function ε_i. In the limit as the width of the damping layer goes to zero the OWWEs are imposed only at the boundary. Precisely, the modified equation (2.3) is then replaced by the system of equations:

$$\begin{aligned}
&u_{tt} = c^2(u_{xx} + u_{yy}), && t > 0, 0 < x < 1, 0 < y < 1 \\
&u_t - cu_x = 0, && x = 0 \\
&u_t + cu_x = 0, && x = 1 \\
&u_t - cu_y = 0, && y = 0 \\
&u_t + cu_y = 0, && y = 1, \\
&u(x, y, 0) \text{ given}, \\
&u_t(x, y, 0) = 0.
\end{aligned} \tag{2.4}$$

In this formulation the OWWEs are solved at the boundary and the acoustic wave equation is used to update the solution everywhere on the interior of the domain.

In either formulation, (2.3) or (2.4), the approach of the pseudospectral method is to interpolate the function $u(x, y, t)$ along grid lines in both x and y directions. Derivatives of $u(x, y, t)$, with respect to x and y, are then approximated by the derivatives of the interpolants. In our work we have used both Chebychev and Legendre pseudospectral methods for these spatial derivatives. Because no great advantage was seen for the Legendre method our results emphasize the Chebychev method which allows for implementation via a fast Fourier transform; see Canuto *et al.* [2]. In either case, after spatial discretization, (2.4) is replaced by

$$\text{(a)}\quad u_{tt}(x_i, y_j, t) = c^2(D_{xx}u + D_{yy}u)(x_i, y_j, t), \qquad 1 \le i \le N-1,\ 1 \le j \le M-1,$$

$$\text{(b)}\quad \begin{cases} u_t(0, y_j, t) = c(D_x u)(0, y_j, t), & 0 \le j \le M \\ u_t(1, y_j, t) = -c(D_x u)(1, y_j, t), & 0 \le j \le M \\ u_t(x_i, 0, t) = c(D_y u)(x_i, 0, t), & 0 \le i \le N \\ u_t(x_i, 1, t) = -c(D_y u)(x_i, 1, t), & 0 \le i \le N. \end{cases} \tag{2.5}$$

Here D_x, D_y, D_{xx}, D_{yy}, are first- and second-order differential operators in x and y, respectively [2] and $(Du)(x_i, y_j, t)$ denotes that the operator D is applied to u and evaluated at the grid point (x_i, y_j, t). The degrees of the interpolation in x and y are given by N and M, respectively.

2.2. *Time Discretization*

The choice of an appropriate time scheme for Eqs. (2.5a) and (2.5b) is not trivial. A first approach is to reformulate the whole system (2.5) as a system of first-order differential equations (ODEs) in time,

$$u_t = Au, \quad \text{where } u = \begin{pmatrix} u_x \\ u_t \end{pmatrix}. \tag{2.6}$$

As such it is amenable to solution by any appropriate ODE solver, which also includes the semi-implicit method of Tal Ezer and Kosloff [20]. But in [6], where the well-posedness of (2.6) is considered, Driscoll and Trefethen show that the operator is highly nonnormal and therefore that the eigenvalues of the operator A are not well-conditioned. Consequently, we chose not to use this ODE system. Instead, in our experiments we adopted the standard second-order differencing in time for Eq. (2.5a):

$$u_{ij}^{n+1} - 2u_{ij}^n + u_{ij}^{n-1} = c^2\,\Delta t^2(D_{xx} + D_{yy})u_{ij}^n, \qquad 1 \le i \le N-1, 1 \le j \le M-1. \tag{2.7}$$

Here u_{ij}^n represents the discrete approximation to $u(x_i, y_j, n\Delta t)$, for a stepsize in time, Δt. The error in time is $O(\Delta t^2)$ which may be large compared to the high-order accuracy in space of the pseudospectral spatial approximation. But our numerical experiments show that the temporal error is not a significant problem because the stability requirement limits Δt in relation to the grid sizes in the x- and y-directions by $\Delta t = O(\Delta x_{\min}^2)$ and $\Delta t = O(\Delta x_{\min})$, where $\Delta x_{\min}$ is the minimum grid spacing for the Chebychev and modified Chebychev methods, respectively.

When the spatial derivatives in Eq. (2.5b) are approximated by finite difference approximations the time derivatives are typically approximated by an explicit method in time. Explicit methods can also be derived for the pseudospectral implementation; for example, for the boundary condition at $x = 0$, illustrative of all boundary conditions, Euler's method would take the explicit form

$$u_{0j}^{n+1} = u_{0j}^n + c\Delta t(D_x u)_{0j}^n, \tag{2.8}$$

which is only of first-order accuracy in time. On the other hand, second-order accuracy in time is achievable with the explicit midpoint, or Leapfrog, method,

$$u_{0j}^{n+1} = u_{0j}^{n-1} + 2c\Delta t(D_x u)_{0j}^n, \tag{2.9}$$

But, a stability analysis immediately rules out (2.9) because the stability region of the midpoint method is just the interval $[-1, 1]$ on the imaginary axis, which does not allow for eigenvalues of the spatial operator to have any real part; see below. However, $O(\Delta t^2)$ accuracy in time can also be obtained by the implicit θ-method,

$$u_{0j}^{n+1} = u_{0j}^n + c\Delta t[\theta(D_x u)_{0j}^{n+1} + (1-\theta)(D_x u)_{0j}^n]. \tag{2.10}$$

With $\theta = \frac{1}{2}$ (2.10) is the Crank–Nicholson method. The implicitness does not present an implementation problem if the interior values are updated via (2.7) before (2.10) is applied. In this case, an implicit equation in terms of the boundary values is still obtained but can be solved directly by taking advantage of the forms of $(D_x u)_{0j}^{n+1}$ and $(D_x u)_{Nj}^{n+1}$, expressed as elements of a matrix vector product; see the Appendix.

A necessary, but not sufficient, requirement for the stability of a numerical implementation of an initial boundary value problem is that both interior and boundary schemes are individually stable [21]. The determination of this requirement for pseudospectral approximations is not as straightforward as for finite difference methods. In particular, the usual von Neumann analysis cannot be applied because it relies on a Fourier transformation to demonstrate the preservation of norms in the Fourier space and,

hence, in the spatial domain. Therefore, for pseudospectral methods, it is standard to use an eigenvalue approach to stability. For this one considers the location of the eigenvalues of the differential operator in relation to the stability region of the ODE solver. However, this technique, called "eigenvalue stability," does not always give sufficient conditions for stability. Trefethen [23] discusses how well any requirements deduced from an analysis of the eigenvalues will give reasonable estimates for Lax-stability. Moreover, Reddy and Trefethen [18] show that for first-order operators the pseudospectra give more realistic stability restrictions; see also [24]. For near-normal matrices, however, the pseudospectra do closely approximate the eigenvalues and therefore an eigenvalue analysis is appropriate.

In the next section we present plots of the eigenvalues for the second-order differential operators. Weideman and Trefethen [26] demonstrated that in this case these eigenvalues are not sensitive to the precision of the calculation and, hence, pseudospectra do closely approximate the eigenvalues. Further, the eigenvalues are real and negative with $O(N^4)$ outliers. Therefore stability restrictions on the timestep are of order $O(1/N^2)$, for explicit discretisations of second-order time derivatives. For the boundary operator the spectrum of the first-order operator is important. This operator, however, is far from normal and has eigenvalues in the left half plane, with $O(N^2)$ outliers. It is for this reason that we would not expect the midpoint method to be a viable method. Neither is Euler's method a good choice because it has a stability region, just the circle in the left half plane with radius one and center at $(-1, 0)$, which imposes very severe restrictions on the timestep in order for the $O(N^2)$ outliers of the first-order differential operator to be moved within this circle. On the other hand, the Crank–Nicholson method is A-stable, with stability region incorporating the whole left half plane. Therefore the $O(N^2)$ outliers present no restrictions on the timestep and our experiments use (2.10) with $\theta = \frac{1}{2}$.

3. THE MODIFIED CHEBYCHEV METHOD

One disadvantage of the Chebychev pseudospectral method for the solution of equations (2.1) and (2.2) is the clustering of the grid points near the boundaries. This has the effect of diminishing resolution at the center of the grid and also, in light of the earlier discussion, at the same time, because of this clustering at the boundaries, imposing stricter limitations on the allowable timesteps for stable solutions. Kosloff and Tal Ezer [16] presented a modified Chebychev method for the solution of problems with first-order spatial derivatives. Their approach is very easily extended for application to second-order spatial derivatives, without additional work for the calculation of the derivatives, provided the appropriate coefficient matrices are set up in an initialisation stage. Therefore, employing the same notation as in Kosloff and Tal Ezer [16], suppose that the collocation points are found from the "stretching" of the regular Chebychev collocation points:

$$x_i = g(z_i, \alpha), \quad -1 \le x_i \le 1, 0 \le i \le N, 0 \le \alpha \le 1, \quad (3.1)$$

and

$$z_i = -\cos\left(\frac{i\pi}{N}\right), \quad 0 \le i \le N.$$

Here α is a parameter of a "stretching" function $g(z, \alpha)$. Note that transformation to the interval $0 \le x \le 1$ is an additional trivial linear transformation. Differentiation of a function $f(x)$ is accomplished by making use of the chain rule,

$$\frac{df}{dx} = \frac{dz}{dx}\frac{df}{dz} = \frac{1}{g'(z, \alpha)}\frac{df}{dz}. \quad (3.2)$$

Therefore for first-order differentiation the operator D is replaced by $\tilde{D} = AD$, where A is a diagonal matrix with entries $A_{ii} = 1/g'(z_i, \alpha)$. Second-order differentiation is accomplished by

$$\begin{aligned}\frac{d^2f}{dx^2} &= \frac{d}{dx}\left(\frac{df}{dx}\right) = \frac{dz}{dx}\frac{d}{dz}\left(\frac{df}{dx}\right) \\ &= \frac{1}{g'(z, \alpha)}\left(\frac{1}{g'(z, \alpha)}\frac{d^2f}{dz^2} - \frac{g''(z, \alpha)}{g'(z, \alpha)^2}\frac{df}{dz}\right),\end{aligned} \quad (3.3)$$

and the second-order derivative operator D_2 is replaced by $\tilde{D}_2 = A^2D_2 + BD$, where A^2 is the square of the diagonal matrix A, and B is the diagonal matrix with entries $B_{ii} = g''(z_i, \alpha)/g'(z_i, \alpha)^3$.

In Kosloff and Tal Ezer [16] plots are presented which verify that the eigenvalues of the matrices $\tilde{D}$ are insensitive with respect to perturbations; in other words, the transformation actually serves to condition the spectra of the matrices D. The spectra of the matrices D_2 are, however, much better conditioned than those of D, even without stretching; see Trefethen and Trummer [25]. In particular, the eigenvalues of D_2 are real, negative, and for interpolation at the Chebychev extrema, as here, satisfy

$$\limsup_{N\to\infty} \frac{\rho(D_2)}{N^4} \le \sqrt{11/4725} \approx 0.0482,$$

where $\rho(D_2)$ denotes the spectral radius of D_2. This $O(N^4)$ behaviour of D_2 imposes a severe $O(1/N^2)$ restriction on the time step used in (2.7). In Fig. 1 we plot the eigenvalues of $\tilde{D}_2$ for various N and $\alpha = \cos(j\pi/N), j = 1, 2, 3$, compared with the exact eigenvalues of the operator d^2/dx^2, and

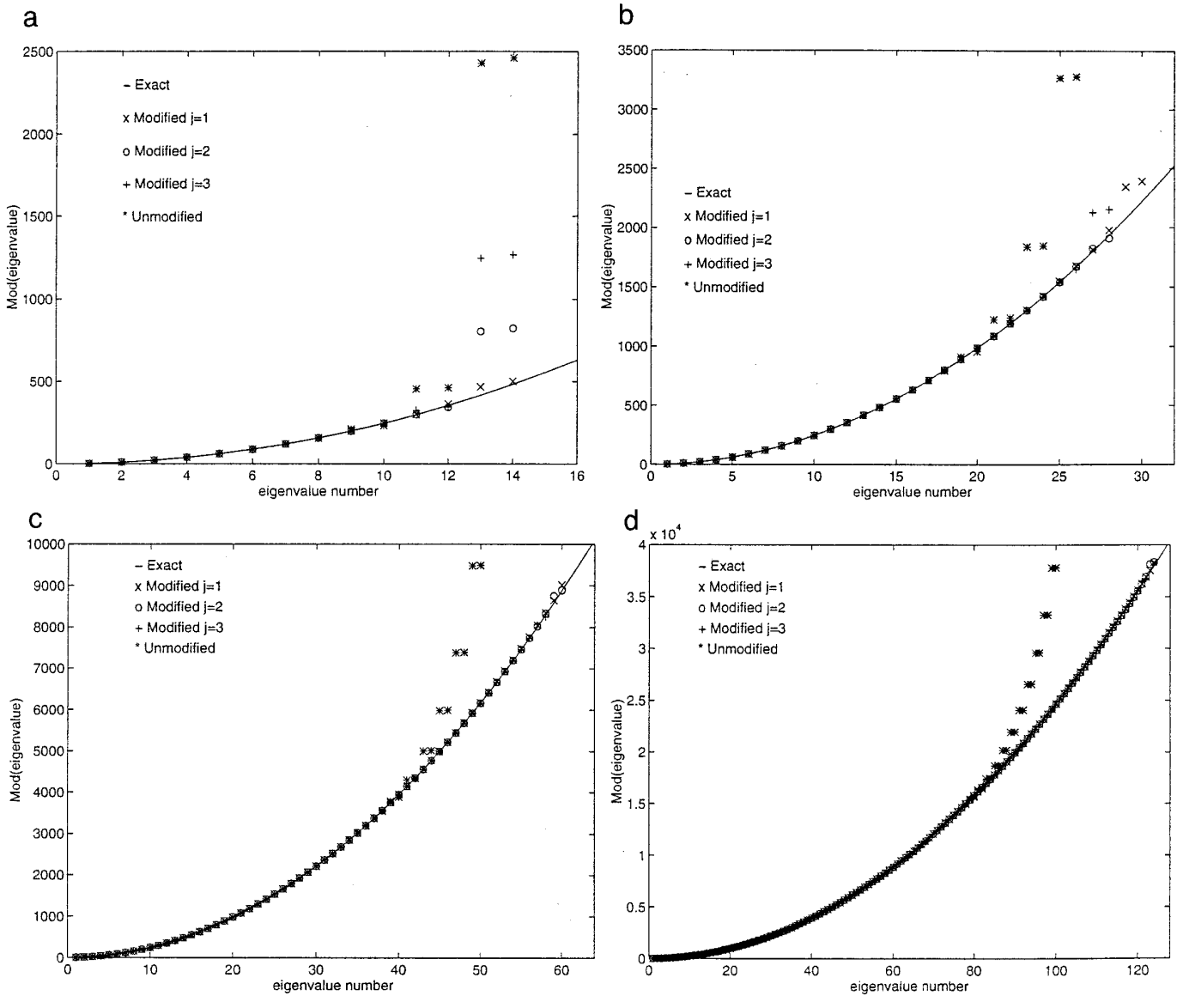

FIG. 1. (a)–(d) Eigenvalues of $\tilde{D}_2$ and D_2, for N = 16, 32, 64, and 128, respectively.

those of D_2. It can be seen that these eigenvalues are again real and negative and that, dependent on α, respectively j, the spectrum more closely approximates that of d^2/dx^2. These results are summarized in Table I. Furthermore, evaluation of both the commutator of $\tilde{D}_2$ and the condition of the matrix of normalised eigenvectors of $\tilde{D}_2$ shows that the matrices $\tilde{D}_2$ are near normal. This is demonstrated in Table II.

In our experiments we chose to use the function $g(z, \alpha) = \sin^{-1}(\alpha z)/\sin^{-1}(\alpha)$ suggested by Kosloff and Tal Ezer [16], with $\alpha = \cos(j\pi/N)$, $j = 1$. Here j represents the number of waves, up to the maximum resolvable, which are not resolved by the grid. For $j = 1$ maximal resolution,

TABLE I

Spectral Radius of the One-Dimensional Second-Order Derivative Operator $\tilde{D}_2$

N	$j = 1$	$j = 2$	$j = 3$	Unmodified
16	5.0E + 02	8.2E + 02	1.3E + 02	2.4E + 03
32	2.4E + 03	4.5E + 03	7.8E + 03	4.4E + 04
50	6.2E + 03	1.2E + 04	2.2E + 04	2.7E + 05
64	1.0E + 04	2.1E + 04	6.1E + 04	7.5E + 05
128	4.4E + 04	9.1E + 04	1.7E + 05	1.2E + 07

TABLE II

Commutator $C(\tilde{D}_2) = \|\tilde{D}_2^T\tilde{D}_2 - \tilde{D}_2\tilde{D}_2^T\|_2/\|\tilde{D}_2^T\tilde{D}_2\|_2$ and Condition $K(M) = \|M\|_2\|M^{-1}\|_2$, of V and $\tilde{V}$, the Matrix of Normalized Eigenvectors of D_2 and $\tilde{D}_2$, Respectively

	$j = 1$		$j = 2$		$j = 3$		Unmodified	
N	$C(D_2)$	$K(V)$	$C(D_2)$	$K(V)$	$C(D_2)$	$K(V)$	$C(D_2)$	$K(V)$
16	5.5E − 02	1.20	1.1E − 01	1.32	1.4E − 01	1.41	1.6E − 01	1.57
32	5.5E − 02	1.21	1.1E − 01	1.34	1.4E − 01	1.46	1.6E − 01	1.89
50	5.5E − 02	1.21	1.1E − 01	1.35	1.4E − 01	1.49	1.6E − 01	2.13
64	5.5E − 02	1.21	1.1E − 01	1.35	1.4E − 01	1.50	1.6E − 01	2.28
128	5.5E − 02	1.21	1.1E − 01	1.36	1.4E − 01	1.52	1.6E − 01	2.74

$r_{\max} = N/2 - 1$, is achieved, where $r_{\max}$ is the maximum wave number resolved by the grid. We note that this choice of α is not necessarily the best choice in terms of accuracy because of the trade-off between accuracy and resolution in space. But, because of stability, it does allow integration in time with a timestep which is significantly larger than that allowed by the Chebychev method, in fact for $N = 128$ a timestep some 16 times larger can be employed; see Table III. In cases where physically the time evolution on the small scale is not required this can lead to an enormous reduction in computational effort. Moreover, we see from the analysis in [16], that as we improve spectral accuracy by increasing j, and consequently decreasing α, the timestep must decrease to maintain stability, and hence the temporal accuracy also improves. An issue in simulations of wave propagation phenomena is the lack of resolution at the center of the grid and, hence, this symmetric transformation, with α near to 1, is the appropriate choice. For models with different boundary conditions at opposite boundaries it may be appropriate to adopt the unsymmetric transformation of Kosloff and Tal Ezer [16]. The transformations suggested by Bayliss and Turkel [1] could also provide reasonable alternatives. In these cases the stability analysis has to be repeated, but the techniques are the same.

4. REFLECTION COEFFICIENTS

In Kosloff and Kosloff [15] a derivation of the reflection coefficient for the modified acoustic wave equation

$$\frac{\partial^2 p}{dt^2} = c^2\frac{\partial^2 p}{dx^2} - 2\gamma\frac{dp}{\partial t} - \gamma^2 p \tag{4.1}$$

is presented. γ is a damping function which is non-zero only at a set of grid points within a predetermined distance of the boundary and is defined by, as used in [15],

$$\gamma = \frac{U_0}{\cosh(\nu \cdot n)^2}, \tag{4.2}$$

where n is the number of grid points of the grid point x_i from the closest boundary. The parameters U_0 and ν determine the width of the boundary layer and how sharply γ tends to zero at the physical boundary. In our two-dimensional experiments we mapped the physical domain onto the domain $[0, 1] \times [0, 1]$, so that the computation was performed on a domain $[-\Delta, 1, +\Delta] \times [-\Delta, 1 + \Delta]$, with the same damping function used at all boundaries.

TABLE III

Observed Stability Limits on $c\Delta t$ for Two-Dimensional Problem

	$j = 1$		$j = 2$		$j = 3$		
N	$c\Delta t$	α	$c\Delta t$	α	$c\Delta t$	α	Unmodified
16	3.1E − 02	.9781	2.4E − 02	.9135	1.9E − 02	.9425	1.4E − 02
32	1.4E − 02	.9949	1.0E − 02	.9795	8.0E − 03	.9541	3.3E − 03
50	9.0E − 03	.9979	6.4E − 03	.9918	4.7E − 03	.9816	1.3E − 03
64	6.9E − 03	.9988	4.8E − 04	.9950	3.6E − 03	.9888	8.1E − 04
128	3.3E − 03	.9997	2.3E − 04	.9988	1.7E − 03	.9972	2.0E − 04

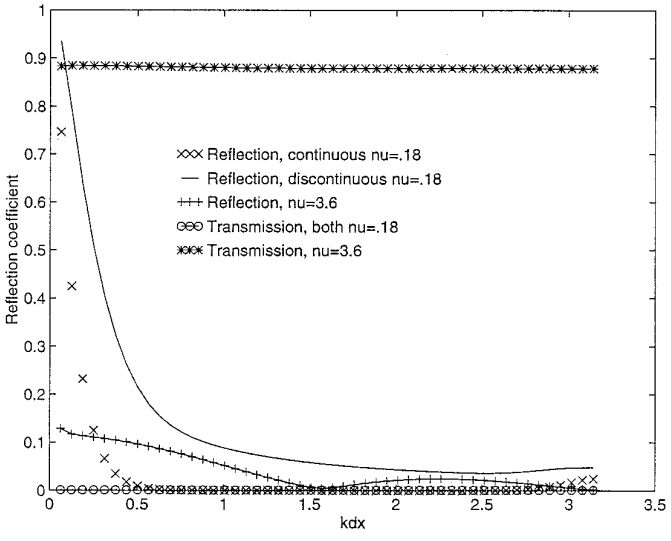

FIG. 2. Comparison of damping layer functions.

For the one-dimensional analysis of the reflection coefficient we make the equivalent assumptions for the solution of (4.1).

The reflection coefficient for a plane sinusoidal wave $e^{-ikx}e^{i\omega t}$ incident from the left on the physical boundary at $x = 1$ can be calculated using the propagator matrix method of Haskell [9]. The application of this method to the determination of the reflection coefficient is well-described in [15] and only necessary ideas are given here.

The idea of the propagator method is to divide the region in which γ is nonzero, $1 \le x \le 1 + \Delta$, into small intervals on each of which γ is taken to be constant. Within each interval there is both a left- and a right-travelling wave, each of different amplitude, which are propagated according to the underlying partial differential equation. Suppose that a wave of unit amplitude is incident at $x = 1$. Ideally the reflected left-travelling wave has an amplitude $R \approx 0$. In practice, R is determined via the solution of successive transmission–reflection problems on each subinterval, which, in turn, by periodicity, depend on the amplitudes of the left- and right-travelling waves at $x = 0$, at which it is assumed the left travelling wave has amplitude zero. But the right travelling wave is transmitted back into the interior domain with an amplitude, T, hopefully near zero. Hence, ideally, not only should we have $R \approx 0$ but also $T \approx 0$, so that no reentrant waves are noticeable at the opposite boundary. Furthermore, the effects of the boundary layer should not extend into the interior, so that the function γ should be negligible on the interior.

In Fig. 2 we present calculations of the reflection and transmission coefficients, R and T, respectively, for different choices of γ. Our numerical experiments in Section 5 have been designed to permit a comparison with the work of Kosloff and Kosloff [15], and therefore the theoretical results are provided to support these experiments. In particular, in [15] a grid with $N = 64$ and a damping layer over 15 grid points were used. There, the damping layer was obtained by choosing $\nu = 0.18$ with $U_0 = 40$ in (4.2). But, in order to have a damping layer over 15 grid points with this choice of γ, there is a discontinuity in γ at the damping layer boundary, $\gamma(0) = \gamma(1) \cong 12.8$, $|\gamma(x)| = 0$, $x \in (0, 1)$. This is a compromise chosen in [15] to fulfill the following contradictory requirements: For fixed width of the layer transition is small if the integral of γ is large and if the gradient of γ is small the reflection is small. However, if γ has to increase from zero at the edge of the layer to a significant value and go back to zero at the other edge there has to be some gradient and, hence, reflection. The difficult task is now to find a shape that meets both requirements. The problem of the damping layer approach resides in the fact that this can not, by construction, be completely achieved, even in the 1D case. In order to illustrate what happens when γ is chosen in a wrong way we report numerical computations when $\nu = 3.6$ and $\nu = 0.18$, for $U_0 = 40$ but in the latter case the damping layer is not restricted to 15 grid points. The corresponding reflection and transmission coefficients are depicted in Fig. 2 and compared with the choice in [15]. Observe that with the latter choice transmission can be successfully suppressed but at the price of admitting some reflection, in particular for small wavenumbers. For the extreme choice $\nu = 3.6$ the transmission is unacceptably high. The numerical calculations confirm these theoretical predictions.

We conclude from this analysis that damping layers, as a means for absorbing waves at artificial boundaries, must be used with caution in the Fourier method. With a careful choice of the damping function the resulting reflection and transmission may be negligible. But our numerical results have shown cases in which reflection or transmission to the opposite boundary may be significant, particularly if the initial signal is close enough to the damping layer boundary. This has severe consequences in terms of memory requirements, in particular, for three-dimensional problems.

On the contrary, however, the Chebyshev-pseudospectral method can be successfully applied without the computational and memory overhead of a damping layer if a first-order absorbing boundary condition is used at the artificial boundary. Because the Chebychev method can also be implemented with the use of fast Fourier transforms its implementation does not require a significant increase in cost as compared to the Fourier-pseudospectral method. Consequently, the non-periodic discretisation without the damping layer presents a much more efficient and robust method for the solution of wave propagation problems. In the next section our numerical results verify these conclusions.

5. NUMERICAL RESULTS

First we give an overview of the numerical tests which have been carried out. Acoustic wave propagation can be modelled by the periodic Fourier pseudospectral solution of the modified acoustic wave equation (4.1), where γ is given by (4.2). This is the method of [15] and has been implemented as a reference. But the model given by (4.1) is not limited to a periodic formulation and we have also solved it using a Chebychev pseudospectral implementation. This implementation, however, does not succeed in removing the entire energy of the incident wave at the boundary, because even in the one-dimensional case there is still a certain amount of reflection at the physical boundary. Furthermore, it requires additional cost due to the presence of the damping layer. For these two reasons this Chebychev implementation is outperformed by the Chebychev implementations described below.

Before continuing with non-periodic formulations we also observe that a Fourier pseudospectral implementation of the modified equation (2.3) would also be possible. Regardless of the appearance of discontinuities in the coefficients, this does not make sense, however. The construction of (2.3) aims at achieving zero reflection and, at the same time, full transmission at these boundaries. Due to the wraparound effect of the periodic formulation the solution would be subject to the same deleterious transmission of waves through opposite boundaries, as argued in the previous section.

The solution of (2.3) with a non-zero thickness OWWE damping layer by a pseudospectral Chebychev discretisation does, however, lead to satisfactory results. Our computations show that this still remains true in the limit where this layer goes to zero and the OWWEs are imposed only at the boundary points, leading to (2.5). Furthermore, the latter computations are more efficient, requiring not only a less dense grid but also allowing a direct implementation of the implicit Crank–Nicholson discretisation of the boundary operators. Therefore, this is the approach which has been retained and for which results are given here.

Legendre pseudospectral discretisations can also be used, but they give very similar results to the Chebychev series. In particular, the stability results are much the same, exhibiting again critical timesteps of $O(1/N^2)$). The modified Chebychev discretisation described in Section 3 overcomes this restriction and leads to the third set of results described in the following paragraphs.

In order to allow comparison between the Fourier and Chebychev pseudospectral methods the physical region was always taken as $[0, 1] \times [0, 1]$ and in all cases it is only this physical region which is plotted. To also allow comparison with the results presented by Kosloff and Kosloff [15], calculations with the Fourier method were done for a 64×64 grid, and a damping layer of 15 grid points. Note that for the Fourier method applied to a physical interval $[x_L, x_R]$ periodicity means that numerically grid points are on the interval $[x_L, x_R - \Delta x]$. In contrast, for a Chebychev grid the whole physical interval is used. Therefore, the Fourier 64×64 grid actually corresponds, by periodicity, to a 65×65 grid, and, with a damping layer of effective width 15 grid points, is equivalent to a Chebychev grid 50×50. The effective grid on the physical region is then 50×50 in both cases. The acoustic velocity was taken as 2, in dimensionless units, equivalent to the 2000 ms^{-1} used in [15]. Simulations with an internal layer of reduced sound velocity, equivalent to the embedded velocity layer simulations in [15], were also carried out, using a local dimensionless acoustic velocity of 1.2. The damping layer was also set up using Eq. (4.2) as indicated in Section 4. To give an effective damping layer over 15 grid points the parameters $U_0 = 40$ and $\nu = 0.18$ were chosen, but, as indicated in Section 4, with the discontinuity in γ at the internal damping layer boundary.

For both the Fourier and scaled Chebychev methods a dimensionless timestep $\Delta t = 0.0045$, near the stability limit for both methods, was used. To maintain stability of the unscaled Chebychev method the timestep was reduced to 0.0006. Measurements were made at equivalent dimensionless times in all cases.

The simulations were initiated with pulses of the form

$$u(x, y, 0) = e^{-r^2 a},$$

where $r^2 = (x - x_0)^2 + (y - y_0)^2$ for an initial pulse centered at (x_0, y_0). For Figs. 4 and 7 the pulse was initiated at the center of the domain, $(x_0, y_0) = (0.5, 0.5)$, and for Fig. 5 the pulse was moved nearer the corner, $(x_0, y_0) = (0.1, 0.1)$. In all cases, the weighting in the pulse was taken to be $a = 500$. Other choices give qualitatively similar results, but require longer time simulations on larger domains to elucidate the results.

The results are illustrated in Fig. 3–7. In Figs. 3a and 3b we present a comparison of the performance of the Fourier method with the different γ functions, by plotting the evolution of the pulse on the domain as measured by the L_2 norm over the physical part of the grid. Here the three choices of γ discussed in Section 4 are used. Namely, (i) $\nu = 0.18$, $U_0 = 40$ with the discontinuity in γ at the damping layer boundary, (ii) $\nu = 0.18$, $U_0 = 40$, but with the function γ going continuously to zero away from the damping layer, and (iii) $\nu = 3.6$, $U_0 = 40$. For Fig. 3a a pulse is initiated at the center of the domain and in Fig. 3b it is initiated at the corner. The effect of $\gamma \neq 0$ on the interior is, as expected, that the pulse is overdamped on the interior domain. On the other hand, the high transmission of the $\nu = 3.6$ case is also verified. Although the discontinuous choice for γ does give the better results and is used in the comparisons with the Chebychev methods,

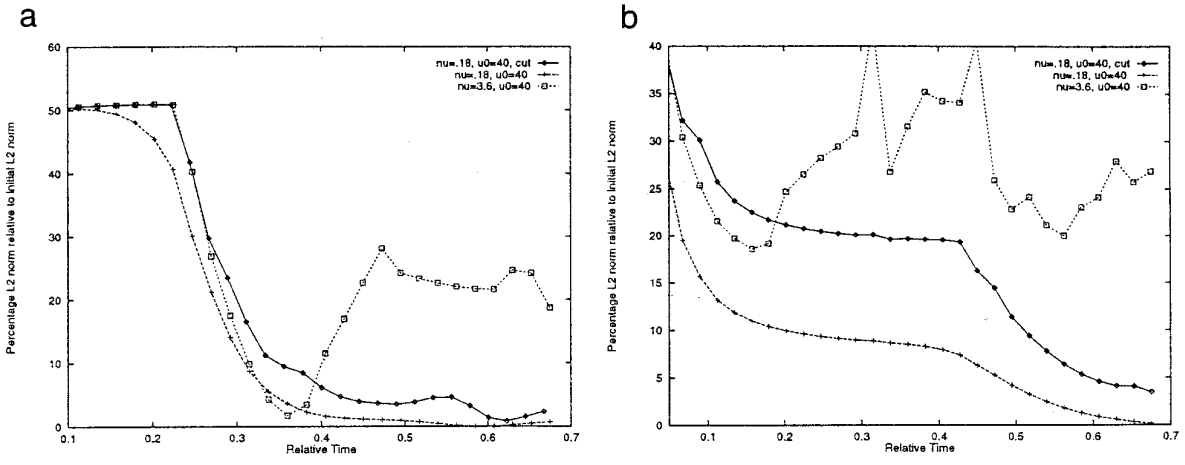

FIG. 3. Comparisons of "energy" for a pulse initiated (a) at the center and (b) at the corner, respectively.

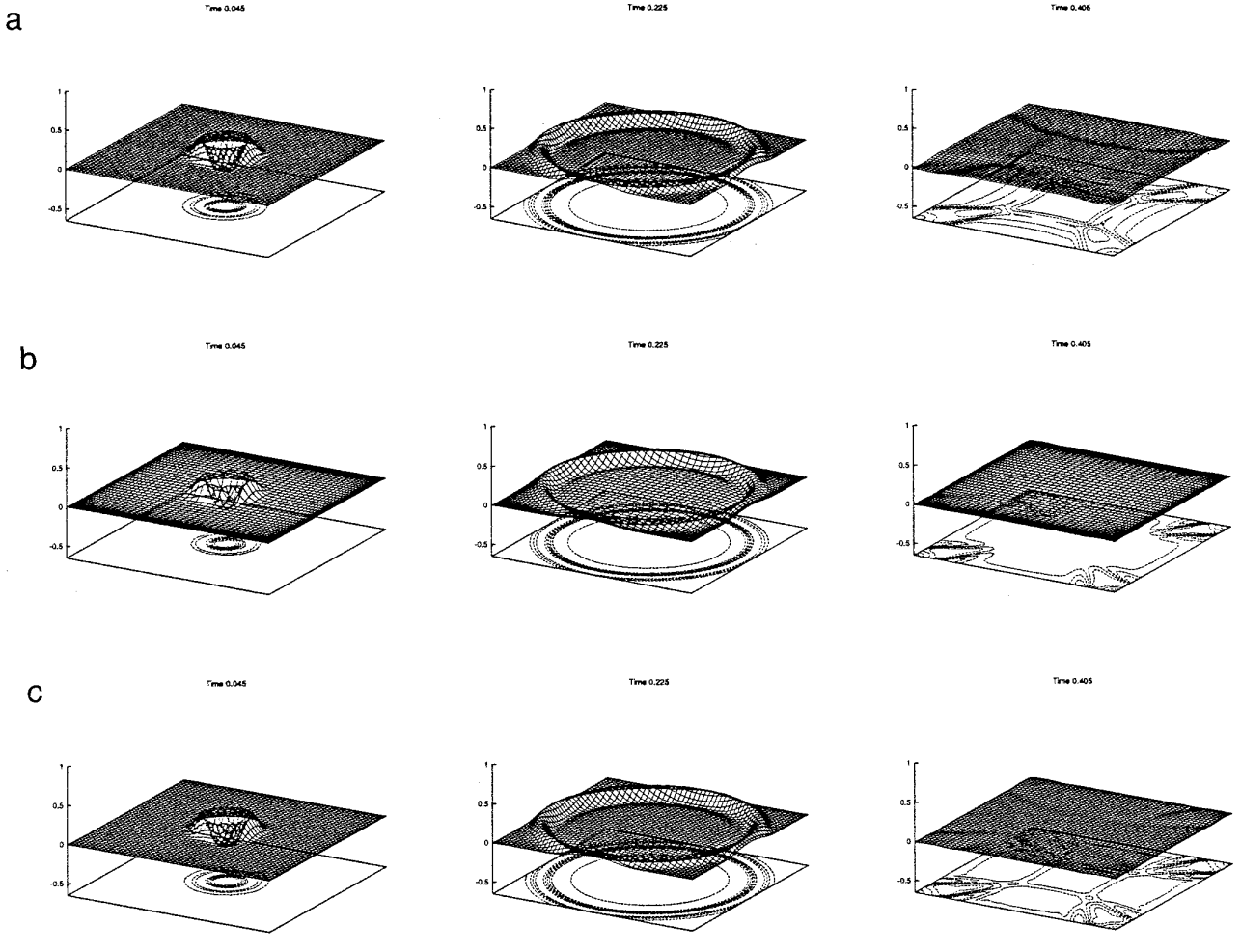

FIG. 4. (a) Fourier for modified Kosloff equation (4.1). (b) Chebychev for acoustic wave with absorbing boundary (2.4). (c) Modified Chebychev for acoustic wave with absorbing boundary (2.4).

we also see that the discontinuity does give rise to greater reflection than is desirable.

Figure 4 shows the evolution of a pulse placed in the center of the grid until it has propagated out of the physical region, with a constant velocity of 2.0. The performance of all three methods is apparent, with in all cases some residual reflection evident. This is most easily observed by examining the contour plots associated with each result. In particular it can be seen in all cases that there are significant corner effects where reflection at two boundaries meeting in a corner causes superposition of the two reflections and hence the increased reflection observed in the contours emanating from the corners. In finite-difference methods these effects are alleviated by the use of special corner conditions applied at the corner and for a few points near the corner. The same adjustments could also be considered in this case. Figures 4b, 5b, and Figures 4c, 5c show a comparison between the two extremes of the Chebychev implementations, i.e., high accuracy but resolution restricted in the center of the grid for Chebychev, as compared to the modified Chebychev, $j = 1$, with high resolution but reduced accuracy.

To allow comparison of these simulations we also plot in Fig. 6, as in Fig. 3, the L_2 measure of how the pulse evolves on the domain. From Fig. 6a we see that the Fourier and Chebychev methods perform nearly identically until the pulse leaves the physical region and the greater reflection of the Fourier method is evident. For simulations over longer time periods the Chebychev methods continue to show negligible energy but the Fourier energy oscillates over time until the wave is eventually completely attenuated over the damping layer. Figure 6b very clearly shows that the discontinuity in $\gamma(x)$ at the physical boundary leads to a reflection of the pulse when it is initiated very close to the physical boundary. We have seen that this can be reduced by taking a much wider damping layer, so that

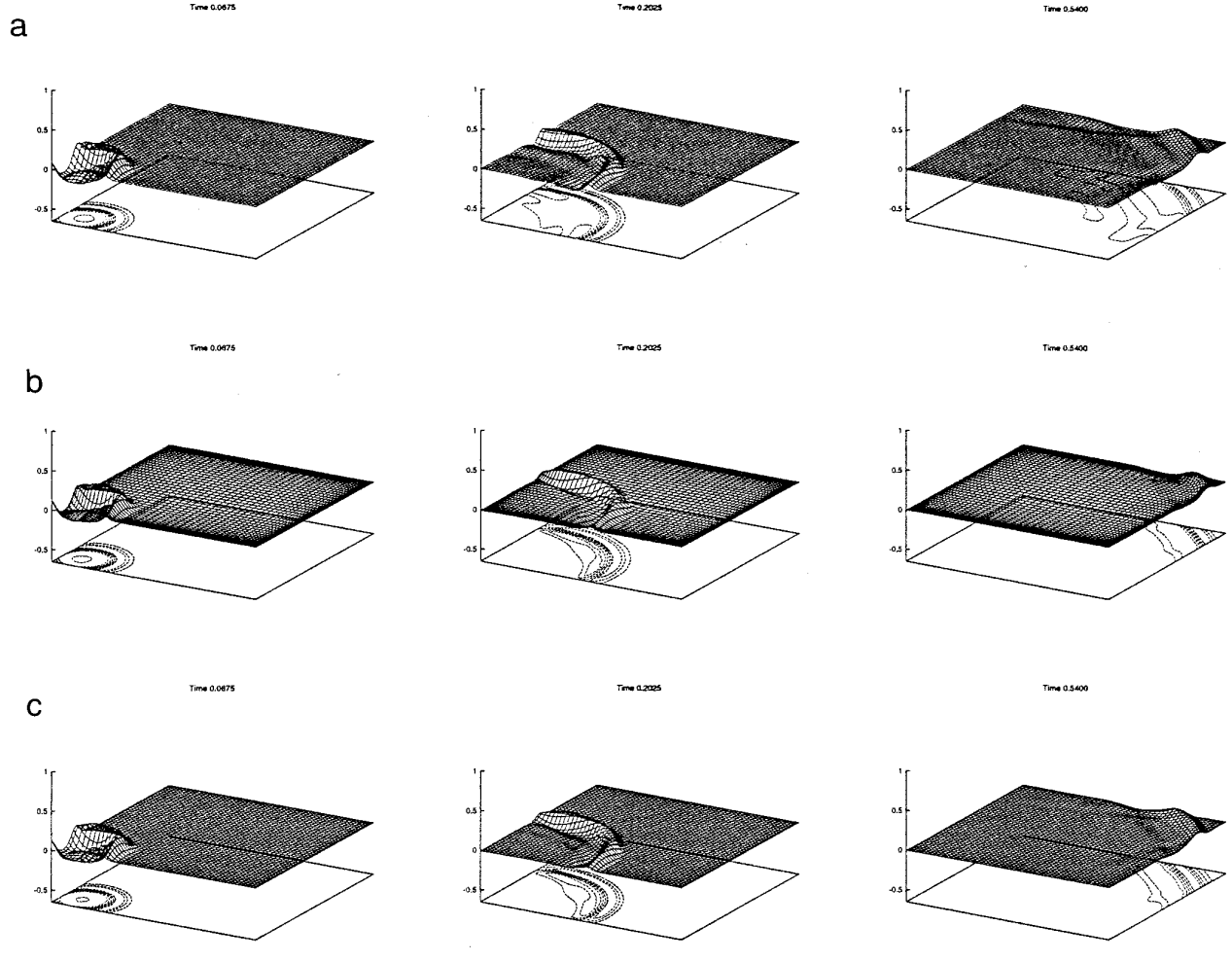

FIG. 5. (a) Fourier for modified Kosloff equation (4.1). (b) Chebychev for acoustic wave with absorbing boundary (2.4). (c) Modified Chebychev for acoustic wave with absorbing boundary (2.4).

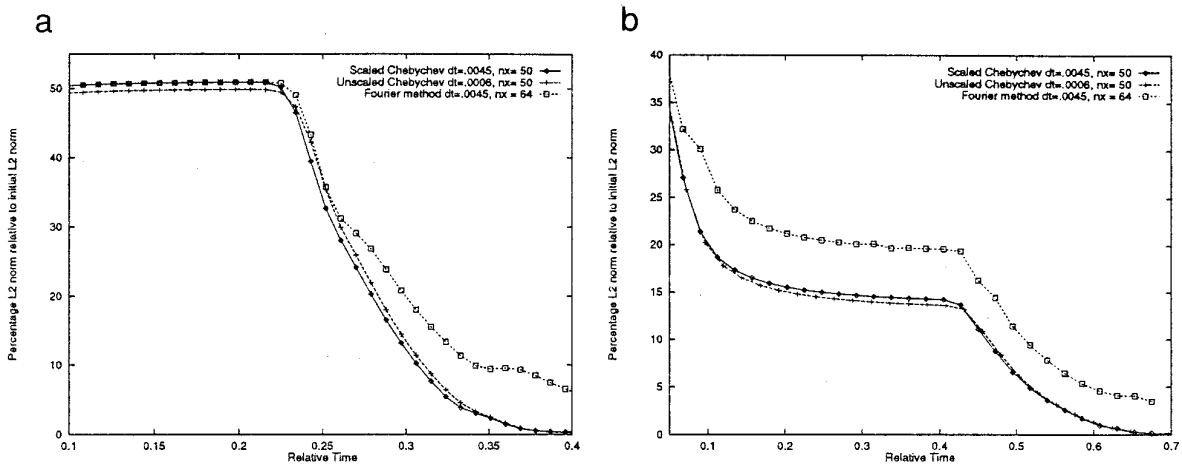

FIG. 6. Comparisons of "energy" for a pulse initiated (a) at the center and (b) at the corner, respectively.

the discontinuity in $\gamma(x)$ is eliminated and the resulting L_2 curve follows that of the Chebychev simulations.

We conclude with a test problem more oriented towards applications, the embedded velocity layer discussed in [15]. The layer of lower sound velocity is oriented parallel to the y-axis (directed away from the spectator in perspective views) and situated just right of center, having a width of four grid points in the Fourier discretisation. Note that the discontinuity in sound velocity can easily be accounted for in the OWWE by modifying the value of c in (2.4). Figure 7 shows a comparison of the solutions obtained with the three methods discussed. We observe that despite the jump in the coefficient the pseudospectral methods behave quite well for this problem. The results also demonstrate that the

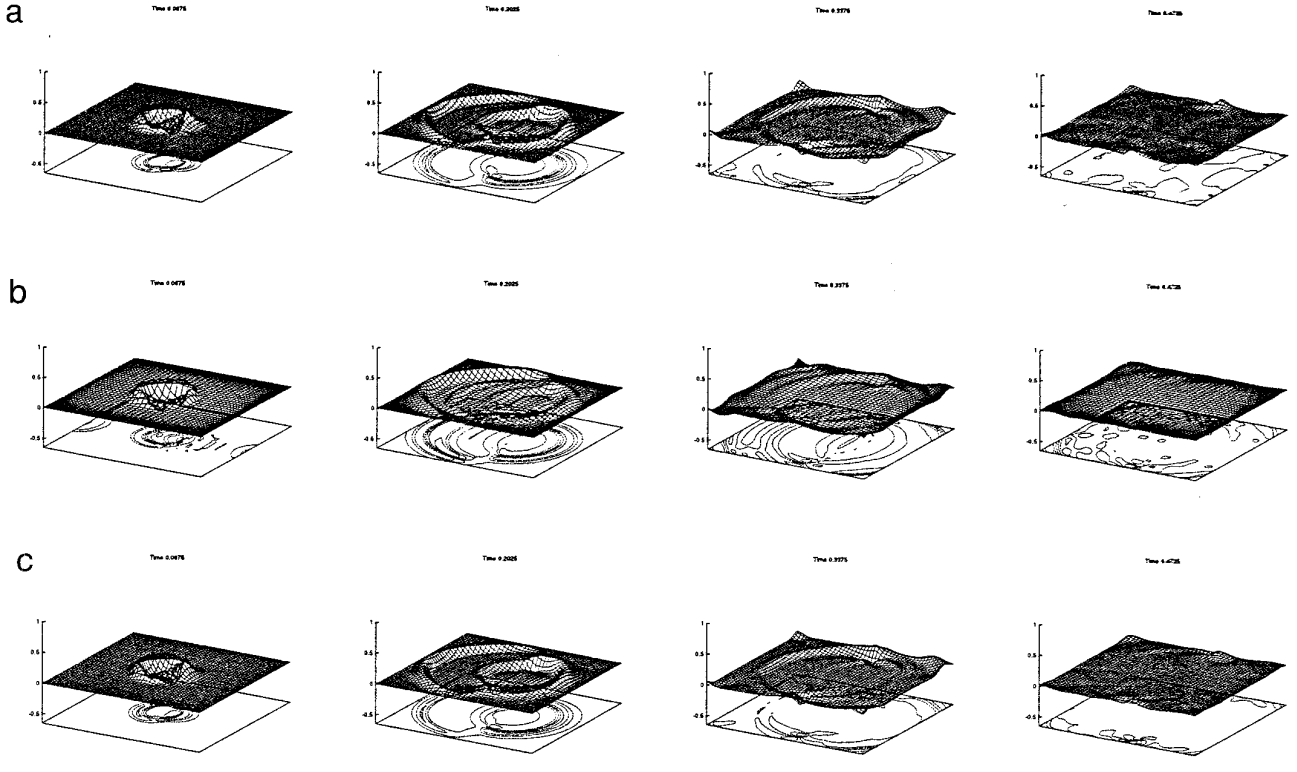

FIG. 7. (a) Fourier for modified Kosloff equation (4.1). (b) Chebychev for acoustic wave with absorbing boundary (2.4). (c) Modified Chebychev for acoustic wave with absorbing boundary (2.4).

present OWWE-formulation for the absorbing boundary is still successful.

Stability limits on $c\Delta t$ for all these two-dimensional simulations are given in Table III and verify that the modified method can proceed with timesteps of the same size as those used for standard Fourier pseudospectral simulations.

6. CONCLUSIONS

A method for the simulation of wave propagation on an artificially bounded domain has been described. The approach is novel in that commonly used OWWEs are incorporated in a non-periodic pseudospectral solution of the acoustic wave equation formulated as a second-order PDE. As such, the formulation allows the high spatial accuracy of pseudospectral methods which leads to negligible numerical dissipation and makes this type of method particularly interesting for the computation of wave propagation phenomena. Compared to periodic Fourier discretisations the non-periodic approach first of all allows zero normal reflection at the boundary, a topic we have discussed in detail. Second, it can be used with similarly sized time steps when employing a "stretching" transformation of the Chebychev points. Finally, these kinds of methods exhiit flexibility with respect to the particular conditions which can be imposed on the boundary and domain decomposition. The discretization in space and time of the Chebychev implementation has been fully addressed. Of particular note is that we have also demonstrated the high spectral accuracy of the spatial transformation for second derivative operators.

Future directions of this research are immediately suggested by the following observations. Because the boundary conditions are implemented directly by the solution of given boundary equations, not only is the technique obviously extendable to three dimensions, but also it is not necessary that all boundaries use the same boundary conditions. A particularly interesting option would be the simulation of surface waves at the surface boundary. Furthermore, improved absorption at an absorbing boundary can be achieved by the implementation of higher-order OWWEs. Moreover, because the boundary operator is one-dimensional, the OWWEs can also be used for media with heterogeneities parallel to the boundary, but constant perpendicular to the boundary. This has been aptly demonstrated for finite difference models by Higdon [12].

APPENDIX: IMPLEMENTATION OF THE CRANK–NICHOLSON METHOD AT THE BOUNDARY

Suppose that absorbing boundary conditions are applied at both the $x = 0$ and $x = 1$ boundaries:

$$\begin{aligned} &\frac{\partial u}{\partial t} - c_1 \frac{\partial u}{\partial x} = 0 \quad \text{at } x = 0 \\ &\frac{\partial u}{\partial t} + c_2 \frac{\partial u}{\partial x} = 0 \quad \text{at } x = 1. \end{aligned} \tag{A1}$$

Here c_1 and c_2 represent the wave propagation speeds at the left and right boundaries, respectively. For simplicity, in the derivation of the scheme, we assume $\theta = \frac{1}{2}$. Extension to arbitrary θ is immediate. At the left boundary, $x = 0$, the Crank–Nicholson scheme corresponds to

$$u_0^{n+1} = u_0^n + c_1 \frac{\Delta t}{2} [(Du)_0^{n+1} + (Du)_0^n], \tag{A2}$$

where $(Du)_0^n = \sum_{j=0}^N d_{0j} u_j^n$ and D is the matrix of the first-order differential operator d/dx, with entries d_{ij}. Because we assume that the values of u_{ij}^n are updated at the interior grid points prior to update of the boundaries, Eq. (A2) is implicit in u_N^{n+1} and u_0^{n+1} only:

$$(Du)_0^{n+1} = d_{00} u_0^{n+1} + d_{0N} u_N^{n+1} + \sum_{j=1}^{N-1} d_{0j} u_j^{n+1}.$$

Therefore, with $k_1 = c_1 \Delta t/2$,

$$(1 - k_1 d_{00}) u_0^{n+1} - k_1 d_{0N} u_N^{n+1} = b_0^n, \tag{A3}$$

where $b_0^n = u_0^n + k_1 \left[\sum_{j=1}^{N-1} d_{0j} u_j^{n+1} + (Du)_0^n\right]$ is known. Equivalently, the equation at the right-hand boundary is

$$\begin{aligned} k_2 d_{N0} u_0^{n+1} + (1 + k_2 d_{NN}) u_N^{n+1} &= b_N^n \\ &= u_N^n - k_2 \left[\sum_{j=1}^{N-1} d_{Nj} u_j^{n+1} + (Du)_N^n\right], \end{aligned} \tag{A4}$$

where $k_2 = c_2 \Delta t/2$. Equations (A3) and (A4) represent a set of two linear equations in two unknowns, u_0^{n+1}, u_N^{n+1},

$$A \begin{pmatrix} u_0^{n+1} \\ u_N^{n+1} \end{pmatrix} = \begin{pmatrix} b_0^n \\ b_N^n \end{pmatrix} = b^n,$$

where

$$A = \begin{pmatrix} 1 - k_1 d_{00} & -k_1 d_{0N} \\ k_2 d_{N0} & 1 - k_2 d_{NN} \end{pmatrix}.$$

For both the Chebychev and the modified Chebychev pseudospectral methods the entries of the differential operator D are such that $d_{00} = d_{NN}$ and $d_{0N} = -d_{N0}$, see [2, p.

69]. Therefore,

$$A = \begin{pmatrix} 1 + k_1 d_{NN} & k_1 d_{N0} \\ k_2 d_{N0} & 1 + k_2 d_{NN} \end{pmatrix}$$

and it immediately follows that

$$u_0^{n+1} = \frac{1}{|A|}((1 + k_2 d_{NN}) b_0^n - k_1 d_{N0} b_N^n),$$

$$u_N^{n+1} = \frac{1}{|A|}(-k_2 d_{N0} b_0^n + (1 + k_1 d_{NN}) b_N^n),$$

where $|A|$ represents the determinant of A.

ACKNOWLEDGMENTS

Part of this work was done at the University of Kaiserslautern. The first author was supported by the Sophia Kovaleskja Chair and the second author by a DFG grant.

REFERENCES

1. A. Bayliss and E. Turkel, *J. Comput. Phys.* **101,** 349 (1992).
2. C. Canuto, M. Y. Hussaini, A. Quarteroni, and T. A. Zang, *Spectral Methods in Fluid Dynamics* (Springer-Verlag, New York/Berlin, 1987).
3. J. M. Carcione, *Numer. Methods Partial Diff. Equations* **10,** 771 (1994).
4. C. Cerjan, D. Kosloff, R. Kosloff, and M. Reshef, *Geophysics* **50,** 705 (1985).
5. R. Clayton and B. Engquist, *Bull. Seismol. Soc. Am.* **67,** 1524 (1977).
6. T. A. Driscoll and L. N. Trefethen, Cornell University, 1993 (unpublished).
7. B. Engquist and A. Majda, *Comm. Pure Appl. Math.* **32,** 313 (1979).
8. L. Halpern and L. N. Trefethen, *J. Accoust. Soc. Am.* **84,** 1397 (1988).
9. N. A. Haskall, *Bull. Seismol. Soc. Am.* **43,** 17 (1953).
10. R. L. Higdon, *Math. Comput.* **47,** 437 (1986).
11. R. L. Higdon, *Math. Comput.* **49,** 65 (1987).
12. R. L. Higdon, *J. Comput. Phys.* **101,** 386 (1992).
13. D. A. Kopriva, FSU-SCR1-92C-17, Florida State University, 1992 (unpublished).
14. D. D. Kosloff and E. Baysall, *Geophysics* **47,** 1402 (1982).
15. R. Kosloff and D. Kosloff, *J. Comput. Phys.* **63,** 363 (1986).
16. D. Kosloff and H. Tal Ezer, *J. Comput. Phys.* **104,** 457 (1993).
17. D. Kosloff, D. Kessler, A. Q. Filho, E. Tessmer, A. Behle, and R. Strahilevitz, *Geophysics* **55**(6), 734 (1990).
18. S. C. Reddy and L. N. Trefethen, *Comput. Methods Appl. Mech. Eng.* **80,** 147 (1990).
19. R. A. Renaut, *J. Comput. Phys.* **102,** 236 (1992).
20. H. Tal Ezer and R. Kosloff, *J. Chem. Phys.* **81,** 3967 (1984).
21. J. C. Strikwerda (Wadsworth & Brooks/Cole, Belmont, CA, 1989).
22. E. Tessmer and D. Kosloff, *Geophysics* **59**(3), 464 (1994).
23. L. N. Trefethen, in *Numerical Methods for Fluid Dynamics III,* edited by K. W. Morton and M. J. Baines (Clarendon Press, Oxford, 1988).
24. L. N. Trefethen, in *Numerical Analysis, 1991,* edited by D. F. Griffiths and G. A. Watson (Longman, New York, 1992).
25. L. N. Trefethen and M. R. Trummer, *SIAM J. Numer. Anal.* **24,** 1008 (1987).
26. J. C. Weiderman and L. N. Trefethen, *SIAM J. Numer. Anal.* **25**(6), 1279 (1988).